Published in final edited form as:
IEEE Trans Med Imaging. 2006 March ; 25(3): 369–375.

Displacement and Velocity of the Coronary Arteries: Cardiac and Respiratory Motion

Guy Shechter,
The Laboratory of Cardiac Energetics, National Institutes of Health, (NHLBI), Department of Health and Human Services (DHHS), Bethesda, MD 20892 USA, and the Department of Biomedical Engineering, Johns Hopkins University, Baltimore, MD 21205 USA. He is now with Philips Research USA, 345 Scarborough Rd., Briarcliff Manor, NY 10510 USA.

Jon R. Resar, and
The Division of Cardiology, School of Medicine, Johns Hopkins University, Baltimore, MD 21205 USA.

Elliot R. McVeigh
The Laboratory of Cardiac Energetics, National Institutes of Health, (NHLBI), Department of Health and Human Services (DHHS), Bethesda, MD 20892 USA.

Abstract

This paper presents measurements of three-dimensional (3-D) displacements and velocities of the coronary arteries due to the myocardial beating motion and due to breathing. Data were acquired by reconstructing the coronary arteries and their motion from biplane angiograms in 10 patients. A parametric motion model was used to separate the cardiac and breathing motion fields. The arteries move consistently toward the left, inferior, and anterior during a cardiac contraction. The displacement and velocity of the right coronary artery during a cardiac contraction was larger than measured for the left coronary tree. Cardiac motion dominates the respiratory motion of the coronary arteries during spontaneous breathing. On inspiration, the arteries move caudally, but the motion in the left-right and anterior-posterior axes was variable. Spatial variation in respiratory displacement and velocity of the coronary arteries indicates that the breathing motion of the heart is more complex than a 3-D translation.

Keywords

Chest imaging; coronary arteries; motion; X-ray angiography

I. Introduction

MOTION during computed tomography (CT) or magnetic resonance (MR) imaging generates artifacts that degrade image quality [1], [2]. Gating techniques are routinely used to “freeze” the heart for cardiac imaging [3]. The beating motion of the heart is compensated by synchronizing the image acquisition with the electrocardiogram (ECG). When imaging times exceed breath hold durations, respiratory motion needs to be addressed [4].

When gating both the cardiac and respiratory motions concurrently, a low imaging duty cycle can result in scan durations that are clinically impractical. Imaging times can be shortened by

*G. Shechter was with the Laboratory of Cardiac Energetics, National Institutes of Health, (NHLBI), Department of Health and Human Services (DHHS), Bethesda, MD 20892 USA, and the Department of Biomedical Engineering, Johns Hopkins University, Baltimore, MD 21205 USA. He is now with Philips Research USA, 345 Scarborough Rd., Briarcliff Manor, NY 10510 USA..

increasing the amount of data acquired for each gating trigger. However, longer image acquisition windows can introduce motion that would degrade image quality. Yet, if the physiologic motion can be measured or modeled, motion compensation methods can be used to prospectively modify the image acquisition, or to retrospectively correct the acquired data, in order to reduce both motion artifacts and scan times [5].

Improving motion correction techniques for imaging the heart and the coronary arteries requires a better understanding of the natural motion of the heart. The purpose of this study was to measure the three-dimensional (3-D) displacement and velocity of the coronary arteries from free breathing coronary angiograms, and to understand the individual contributions of the cardiac contraction and breathing. This study complements a recently published report on the rest periods of the coronary arteries during the cardiac and respiratory cycles [6].

II. Methods

A. Imaging

Biplane coronary angiograms were acquired using conventional techniques with a Siemens HICOR Angiography system at 30 frames/s. Each angiogram captured 3–6 s of motion including several cardiac cycles and approximately one respiratory cycle of motion. Patients were given no breathing commands to avoid making them conscious of their breathing.

B. Patients

Conventional biplane coronary angiograms were obtained in 8 male and 2 female patients (mean age, 65 ± 11 years) referred for diagnostic left heart catheterization. All patients gave written informed consent to participate in this institutional review board approved study. Four patients had mild dilated cardiomyopathy, and two had mild to moderate hypertrophy.

C. Recovering Coronary Artery Motion

The motion of the arteries was recovered from each biplane angiogram dataset using stereo reconstruction and motion tracking techniques. First, a static 3-D model of the coronary arteries was reconstructed at mid-diastole from one pair of images. The images were processed with filters that enhance the location of arteries [7], and the arterial centerlines were semi-automatically drawn in the two images. Point to point correspondences between the arteries drawn in the two projections were computed automatically and a 3-D model was reconstructed using knowledge of the geometry of the imaging system [8]. Using the static coronary tree model as an initial state, the 3-D motion of the arteries was recovered using an automatic motion tracking algorithm [9]. This algorithm calculates the best 3-D transformation of the reconstructed coronary tree model such that the projection of the arteries remains consistent with the temporally changing image sequence. An energy minimization framework was formulated that uses analytical gradient descent to recover the parameters of the rigid body, affine, and local deformation field that changes the shape of the coronary arteries. Additional constraints were used to ensure a spatially smooth deformation field, and to prevent large changes in the 3-D length of the coronary arteries during their deformation. Validation experiments with a moving vascular phantom demonstrated a reconstruction root-mean square error (RMSE) of 0.66 ± 0.04 mm, and a motion tracking RMSE of 0.69 ± 0.06 mm.

The motion field, $d(\chi,\rho)$, recovered from each dataset represents the arteries while the heart is beating and the patient is breathing. The field is a function of cardiac phase (χ) and respiratory phase (ρ). χ is a measure derived from the ECG that represents the percentage of the cardiac cycle with $\chi = 0$ and $\chi = 1$ corresponding to successive QRS peaks. ρ is calculated from the angiograms by measuring the displacement of the diaphragm-lung interface relative to end-expiration [10]. A profile perpendicular to the diaphragm—lung interface was manually

positioned on a first image, and all the images in a dataset were sampled at this location. The displacement of the diaphragm—lung interface over time generates a one-dimensional (1-D) curve that was manually segmented using a B-spline approximating curve, with the maximum and minimum values corresponding to end-expiration ($\rho = 0$) and end-inspiration ($\rho = \pm 1$) The sign of ρ depends on whether the image is acquired during inspiration (+) or expiration (−).

A parametric cardiac respiratory model was used to decompose the motion field into independent cardiac and respiratory motion components so that

$$d(\chi, \rho) = d_c(\chi) + d_r(\rho) \quad (1)$$

where $d_c(\chi)$ represents only the cardiac contraction, and $d_r(\rho)$ represents the respiratory motion [11]. The functions $d_c(\chi)$ and $d_r(\rho)$ are modeled as periodic B-spline basis functions, and the B-spline control points are optimized so that the model approximates the displacement field recovered from the vessel motion tracking algorithm. The decomposition is made possible with the assumption that the cardiac and respiratory motion fields are independent. These parametric functions are smooth and interpolating in nature, which enables the interpolation of the deformation field at cardiac-respiratory phase combinations other than those seen in the angiogram. After recovering d_c and d_r, these subfields were independently applied to displace the coronary tree models, allowing us to study the cardiac contraction and breathing motions separately.

D. Data Evaluation

The right coronary artery (RCA) was studied in four patients. The RCA was divided into proximal, middle, and distal thirds by an interventional cardiologist [12]. Three points on the RCA were selected for study: 1) RCA_O : the RCA origin; 2) $RCA_{.5AM}$: the point of intersection of the proximal and middle thirds, which is approximately one-half the distance to the acute margin of the heart; 3) RCA_{AM} : the point of intersection of the middle and distal thirds, which is the acute margin of the heart.

The left coronary tree was studied in seven patients. Four landmarks were systematically identified for further study: 1) LM_O : the left main (LM) origin; 2) LM_B : the LM bifurcation; 3) LAD_5 : a point on the left anterior descending artery 5 cm away from the LM origin; 4) LC_{X5} : a point on the left circumflex 5 cm from the LM origin.

The cardiac-only motion field was applied to the 3-D coronary model and mutually orthogonal 1-D displacements were measured along the patient's left-right (LR), inferior-superior (IS), and posterior-anterior (PA) axes. The reference position was end-diastole ($\chi = 0$). Breathing was held fixed at end-expiration by setting a constant $\rho = 0$ and evaluating (1) at different values of χ.

Similarly, respiratory motion was analyzed using the respiration-only motion field, with respect to end-expiration ($\rho = 0$). Cardiac phase was fixed at mid-diastole by setting χ from (1) to a constant. This value was determined independently for each patient by examining the angiogram image sequence and finding the cardiac phase in diastole that had the smallest frame-to-frame motion of the coronary arteries.

Velocities were computed by finite differences of the position measurements. Peak velocity was determined for each patient during three subphases of the cardiac cycle: 1) systole ($0 \leq \chi < 0.42$); 2) the rapid filling phase of early diastole ($0.42 \leq \chi < 0.70$); 3) atrial contraction ($0.80 \leq \chi < 1$). Mean and peak velocities were calculated separately for expiration ($-1 < \chi < 0$) and inspiration ($0 < \chi < 1$)

E. Statistics

Measurements are reported as a mean ± one standard deviation. Displacements and velocities were compared using a two-tailed Student's t-test with significance level of 0.05. The t-test for paired samples was used when comparing results within a patient. Multiple pair-wise comparisons were performed using a Bonferroni t-test [13].

III. Results

A. Cardiac Displacement

Patient-averaged peak 1-D and 3-D displacements of the coronary landmarks during the cardiac cycle are summarized in Table I. As the heart contracts, the motion of the landmarks was consistently toward the patients' left inferior and anterior, with larger magnitudes seen for the RCA. The displacement of the RCA ostium over a cardiac cycle is shown in Fig. 1 for four patients.

The maximum 3-D displacement of the RCA ostium during the cardiac cycle (mean, 14.4 ± 1.9 mm) was significantly less than the peak 3-D displacement of the distal landmarks, $RCA_{.5AM}$ (mean, 26.3 ± 3.1 mm, $P < 0.001$,, Bonferroni t-test with three comparisons), and RCA_{AM} (mean, 23.2 ± 1.6 mm, $P < 0.003$, Bonferroni t-test with three comparisons).

The peak 3-D displacement of the left circumflex landmark during the cardiac cycle (mean, 12.1 ± 2.4 mm) was significantly higher than the peak 3-D displacement of LM_O (mean, 7.9 ± 2.2 mm, $P < 0.001$), LM_B (mean, 8.5 ± 1.7 mm, $P < 0.001$), and LAD_5 (mean, 9.6 ± 1.3 mm, $P < 0.004$, Bonferroni t-test with six comparisons).

B. Respiratory Displacement

Patient-averaged peak 1-D and 3-D displacements of the coronary landmarks over a respiratory cycle are presented in Table II. The magnitude of motion is similar for the right and left coronary arteries, with the heart moving toward the patient's feet from end-expiration to end-inspiration. The direction of motion in the LR and PA axes was more variable. The displacement of the RCA ostium over a tidal respiratory cycle is shown in Fig. 2.

Larger displacements were measured distally along the RCA, where the displacement at RCA_{AM} was statistically larger than at RCA_O ($P < 0.007$, Bonferroni t-test with three comparisons). The displacement at LCx_5 was statistically larger than at LM_O ($P < 0.0001$) and at LM_B($P < 0.002$, Bonferroni t-test with six comparisons).

C. Cardiac Velocity

Patient-averaged peak coronary velocities during the three high-velocity phases of the cardiac cycle are summarized in Table III. The velocity of the left coronary landmarks over a cardiac cycle are plotted in Fig. 3. The profiles are similar to those observed for the RCA, but the magnitude of the velocity was larger for the left coronary.

Distal segments of the RCA had higher velocities than proximal regions. During systole, the peak velocity at $RCA_{.5AM}$ (mean, 130.7 ± 19.4 mm/s) was statistically higher than the peak velocity at the RCA ostium (mean, 69.8 ± 13.8 mm/s, $P < 0.001$, Bonferroni t-test with three comparisons).

The left circumflex had higher velocities than the LM ostium during the cardiac cycle. The peak velocity of LCx_5 during systole was 56.4 ± 10.3 mm/s compared with peak velocity at LM_O of 34.5 ± 8.8 mm/s ($P < 0.0005$, Bonferroni t-test with six comparisons). This statistical

relationship was also observed in the rapid filling phase of early diastole ($P < 0.004$), and the atrial contraction($P < 0.0005$).

D. Respiratory Velocity

Velocity plots of the coronary arteries during a tidal respiratory breath (Fig. 4) show two high-velocity regions corresponding to expiration ($\rho < 0$) and inspiration ($\rho > 0$), bounded by low velocity periods at end-inspiration ($\rho = \pm 1$) and at end-expiration ($\rho = 0$). Patient-averaged peak inspiratory and expiratory velocities are summarized in Table IV.

The peak expiratory velocities measured for the RCA were between 3.3–8.6 mm/s in four patients, with significantly higher peak velocities at the distal landmark RCA_{AM} (mean, 6.4 ± 1.7 mm/s) than at the RCA ostium (mean, 4.5 ± 1.6 mm/s, $P < 0.008$, Bonferroni t-test with three comparisons).

IV. Discussion

The displacement and velocity of the RCA during a cardiac contraction was larger than for the left coronary tree. The RCA is found in the atrio-ventricular groove, located at the base of the heart. Studies of the mechanics of the heart have identified more motion at the base than at the apex. This topographic effect is consistent with the observation that among the left coronary vessels, the circumflex artery, which also follows the atrio-ventricular groove, has larger displacements and velocities.

Cardiac motion dominates the respiratory motion of the coronary arteries. Three-dimensional (3-D) displacements of up to 30 mm were observed in the proximal 7.5 ± 1.1 cm of the RCA. Tidal respiratory motion of the same anatomic region was up to 9.7 mm. In the proximal 5 cm of the left coronary tree—including the left main, left anterior descending, and left circumflex arteries—the maximum 3-D displacement was 16.2 mm due to cardiac motion, and 9.3 mm due to breathing.

The displacement of the coronary arteries was directed caudally on inspiration. The motion in the left-right and anterior-posterior directions was more variable between patients. The direction of motion was unbiased in these two axes, with the standard deviation of the motion larger than the mean. Distal arterial segments showed larger velocities than proximal segments. Spatial variation in respiratory displacement and velocity indicates that the global motion of the heart during breathing is more complex than a 3-D translation. For a given landmark, mean and peak velocities were higher during expiration than during inspiration. This can be explained primarily due to the difference in the duration of the inspiratory and expiratory maneuvers since the overall displacement during the two phases was equal in magnitude.

A. Comparison With Previous Studies: Cardiac Motion

Measurements of coronary motion have been made previously. The majority of the literature contains studies of the cardiac motion of the heart during a breath hold, with fewer reports of respiratory motion of the arteries. Confidence in our results is obtained by comparing them with reports of motion parameters found in these previous works.

A plot of RCA displacement as a function of the cardiac cycle found in [14] (see Fig. 5) is very similar to Fig. 1(d). Saranathan *et al.* acquired MR images with a voxel resolution of 2.8 × 1.4 × 5 mm and reported peak RCA displacements of approximately 15–20 mm. We found a range of 13–17 mm for peak RCA ostium 3-D displacement.

Hofman *et al.* measured the in-plane cardiac motion of the coronary arteries in cross sectional images with a voxel size of 1 × 1.4 × 5 mm [15]. Measurements were reported for four

landmarks that matched closely with the location of our landmarks. They reported maximum in-plane displacements of 25 ± 5 mm for the RCA, 9 ± 1 mm for the LM, 11 ± 4 mm for the LAD, and 12 ± 2 mm for the LCx. Our 3-D measurements were nearly identical: 26 ± 3 mm for the RCA_o, 8 ± 2 mm for LM_o, 10 ± 1 mm for the LAD_5, and 12 ± 2 mm for LCx_5. The close similarities in the two-dimensional (2-D) and 3-D measurements suggests that the choice of imaging planes proposed in [16] may be effective because they minimize the effects of through-plane arterial motion during the cardiac cycle.

The 3-D velocity of the coronary arteries during a cardiac contraction was measured with multislice spiral CT by Vembar *et al.* [17]. Systolic velocities of 47 ± 22 mm/s were reported at the RCA ostium, and 91 ± 42 mm/s at RCA_{AM}. Our data showed the same trend toward higher velocities at distal RCA landmarks, but we found larger velocities (RCA_o = 70 ± 14 mm/s; RCA_{AM} = 102 ± 13 mm/s). For the left coronary tree, they reported systolic velocities of 29 ± 12 mm/s, 24 ± 13 mm/s, and 68 ± 28 mm/s, respectively, at the left main ostium, left anterior descending, and left circumflex arteries. In comparison, our measurements were 35 ± 9 mm/s, 47 ± 9 mm/s, and 57 ± 10 mm/s. The CT reconstruction algorithm generated images every 12.5% of the cardiac cycle by pooling data over a 250-ms window. Temporal smoothing due to long imaging windows could lead to an underestimation of peak velocities.

B. Comparison With Previous Studies: Respiratory Motion

Published reports on the motion of the heart due to breathing used ECG-gated MR imaging to freeze cardiac motion. A discussion of the respiratory displacements reported in the literature follows. To the best of our knowledge there are no reports of coronary velocity during breathing.

Bogren provided the first quantitative study of the respiratory motion of the heart from X-ray cineangiograms [18]. He observed that the superior-inferior (SI) motion at the valve planes was approximately half as much as the SI motion of the diaphragm, which averaged 15 mm (range=10–19 mm) during normal respiration; this reflects an SI motion of the valve planes of 5–10 mm. We reported mean SI displacements of 5.9 ± 3.1 and 5.6 ± 1.5 mm, respectively, for the anterior margin of the right coronary and for the left circumflex artery. These anatomical landmarks are found in the atrio-ventricular groove, which corresponds to the valve plane used by Bogren.

More recently, the few published experimental reports on the motion of the coronary arteries due to breathing have used ECG-gated MR imaging to freeze the effects of cardiac motion. The nature of the MR acquisition has resulted in two general classes of imaging protocols: 1) 2-D and 3-D imaging at multiple breath holds simulating normal breathing; 2) 2-D real time imaging during free breathing. Neither of these methods is suited for measuring 3-D respiratory motion during free breathing. In contrast, the biplane X-ray coronary angiograms used in this study offered higher temporal and spatial resolution images, and using computer vision reconstruction methods, the ability to make 3-D measurements from a single spontaneous breathing cycle.

Wang *et al.* measured the tidal respiratory displacement of the coronary arteries in ten healthy volunteers using 2-D MR imaging with a voxel size of 1.1 × 2.2 × 5 mm [19]. In 10 patients, the displacement of the RCA ostium was 10.5 ± 4.8 mm in the cranio-caudal direction and 2.3 ± 1.4 mm in the anterior-posterior direction. The LAD was reported to move 13.1 ± 4.1 mm and 2.0 ± 0.7 mm in those axes. The cranio-caudal displacements are nearly three times larger than we measured (RCA_o: 4.1 ± 1.6 mm; LAD_5: 4.7 ± 1.8 mm). Wang acquired images during a breath hold, and the tidal respiratory range was sampled by asking the patients to hold their breath at different respiratory positions. The average diaphragmatic displacement was reported to be 20 mm, which is larger than diaphragmatic displacements observed during free breathing.

This suggests that simulated tidal breathing motion would produce larger displacements than we would observe during spontaneous tidal breathing. Results supporting this hypothesis were presented in [20].

Secondly, displacement measurements were made in 2-D images, which raises the concern that the measurements made between two images at different respiratory positions did not track material points. Finally, compared to the 33-ms temporal resolution we obtained with X-ray angiography, the temporal resolution of the MR acquisition was 117 ms, and images were created by combining data acquired over 16 heartbeats. Temporal averaging may have caused displacement from the cardiac contraction, or variances in beat-to-beat motion of the arteries, to be classified as respiratory motion.

LM cranio-caudal displacements of 9 ± 3 mm during tidal respiration were measured using real-time MR imaging in 12 healthy volunteers [21]. Two-dimensional slices with a voxel size of (0.75 – 2.2) × (0.75 – 2.2) × 4 mm were acquired during one 100 ± 10-ms temporal window. These free breathing results are smaller than those reported by Wang, but still larger than our measurements.

McLeish *et al.* reported the respiratory displacement of a point along the RCA using 3-D MR imaging with 25–30 s breath holds [22]. The temporal resolution of the images was 180 ms, and the spatial resolution was 1.4 × 1.4 × 6 mm. The mean displacement was 8.2 ± 3.4 mm in 9 patients, and 17 ± 4.3 mm in 8 volunteers. It is difficult to directly compare the results since the position of their RCA landmark is not known, but their patient results are similar to the 3-D displacements we measured in patients at $RCA_{.5AM}$ (6.4 ± 1.9 mm) and RCA_{AM} (7.2 ± 2.2 mm).

V. Conclusion

Displacement and velocity measurements of the coronary arteries were made from X-ray angiograms. Measurements of displacement during the cardiac cycle correlate well with published measurements obtained during a breath-hold. Measurements of the breathing motion of the heart were smaller than those previously reported with MR techniques that relied on simulated breathing or data averaging across multiple cardiac and respiratory cycles.

References

1. Ritchie C, Godwin J, Crawford C, Stanford W, Anno H, Kim Y. Minimum scan speeds for suppression of motion artifacts in CT. Radiology 1992;185:37–42. [PubMed: 1523332]
2. Wood M, Henkelman R. MR image artifacts from periodic motion. Med. Phys Apr.;1985 12:143–151. [PubMed: 4000069]
3. Lanzer P, Barta C, Botvinick E, Wiesendanger H, Modin G, Higgins C. ECG-synchronized cardiac MR imaging: method and evaluation. Radiology 1985;155(3):681–686. [PubMed: 4001369]
4. Ehman R, McNamara M, Pallack M, Hricak H, Higgins C. Magnetic resonance imaging with respiratory gating: Techniques and advantages. AJR Dec.;1984 143:1175–1182. [PubMed: 6333787]
5. Keegan J, Gatehouse P, Yang G-Z, Firmin D. Coronary artery motion with the respiratory cycle during breath-holding and free-breathing: Implications for slice-followed coronary artery imaging. Magn. Reson. Med 2002;47:476–481. [PubMed: 11870834]
6. Shechter G, Resar J, McVeigh E. Rest period duration of the coronary arteries: implications for magnetic resonance coronary angiography. Med. Phys Jan.;2005 32(1):255–262. [PubMed: 15719976]
7. Frangi A, Niessen W, Hoogeveen R, van Walsum T, Viergever M. Model-based quantitation of 3-D magnetic resonance angiographic images. IEEE Trans. Med. Imag Oct.;1999 18(10):946–956.
8. Mourgues F, Devernay F, Malandain G, Coste-Manière E. 3D+t modeling of coronary artery tree from standard non simultaneous angiograms. Proc. MICCAI Oct.;2001 2208:1320–1322.

9. Shechter G, Devernay F, Coste-Manière E, Quyyumi A, McVeigh E. Three-dimensional motion tracking of coronary arteries in biplane cineangiograms. IEEE Trans. Med. Imag Apr.;2003 22(4): 493–503.
10. Shechter G, Shechter B, Resar J, Beyar R. Prospective motion correction of X-ray images for coronary interventions. IEEE Trans. Med. Imag Apr.;2005 24(4):441–450.
11. Shechter G, Ozturk C, Resar J, McVeigh E. Respiratory motion of the heart from free breathing coronary angiograms. IEEE Trans. Med. Imag Aug.;2004 23(8):1046–1056.
12. Austen W, Edwards J, Frye R, Gensini G, Gott V, Griffith L, McGoon D, Murphy M, Roe B. A reporting system on patients evaluated for coronary artery disease. Circ Apr.;1975 51(4 suppl):5–40.
13. Glantz, S. Primer of Biostatistics. 3rd ed.. McGraw-Hill, Inc.; New York: 1992. p. 309-310.ch. 9
14. Saranathan M, Ho V, Hood M, Foo T, Hardy C. Adaptive vessel tracking: automated computation of vessel trajectories for improved efficiency in 2D coronary MR angiography. J. Magn. Reson. Imag 2001;14:368–373.
15. Hofman M, Wickline S, Lorenz C. Quantification of in-plane motion of the coronary arteries during the cardiac cycle: Implications for acquisition window duration for MR flow quantification. J. Magn. Reson. Imag 1998;8(3):568–576.
16. Post J, van Rossum A, Hoffman M, Valk J, Visser C. Protocol for two-dimensional magnetic resonance coronary angiography studied in three-dimensional magnetic resonance data sets. Am. Heart. J 1995;130:167–173. [PubMed: 7611108]
17. Vembar M, Garcia M, Heuscher D, Haberl R, Matthews D, Bohme G, Greenberg N. A dynamic approach to identifying desired physiological phases for cardiac imaging using multislice spiral CT. Med. Phys Jul.;2003 30(7):1683–1693. [PubMed: 12906185]
18. Bogren H, Lantz B, Miller R, Mason D. Effect of respiration on cardiac motion determined by cineangiography. Acta Radiologica Diagnosis Nov.;1977 18:609–620. [PubMed: 605810]
19. Wang Y, Riederer S, Ehman R. Respiratory motion of the heart: kinematics and the implications for the spatial resolution in coronary imaging. Man. Reson. Med May;1995 33(5):713–719.
20. Keegan J, Gatehouse P, Yang G-Z, Firmin D. Subject-specific motion correction factors for magnetic resonance coronary angiography. Proc. IEEE 2001 Int. Workshop Medical Imaging and Augmented Reality (MIAR) 2001:67–71.
21. Danias P, Stuber M, Botnar R, Kissinger K, Edelman R, Manning W. Relationship between motion of coronary arteries and diaphragm during free breathing: lessons from real—time MR imaging. AJR 1999;172:1061–1065. [PubMed: 10587147]
22. McLeish K, Hill D, Atkinson D, Blackall J, Razavi R. A study of the motion and deformation of the heart due to respiration. IEEE Trans. Med Imag Sep.;2002 21(9):1142–1150.

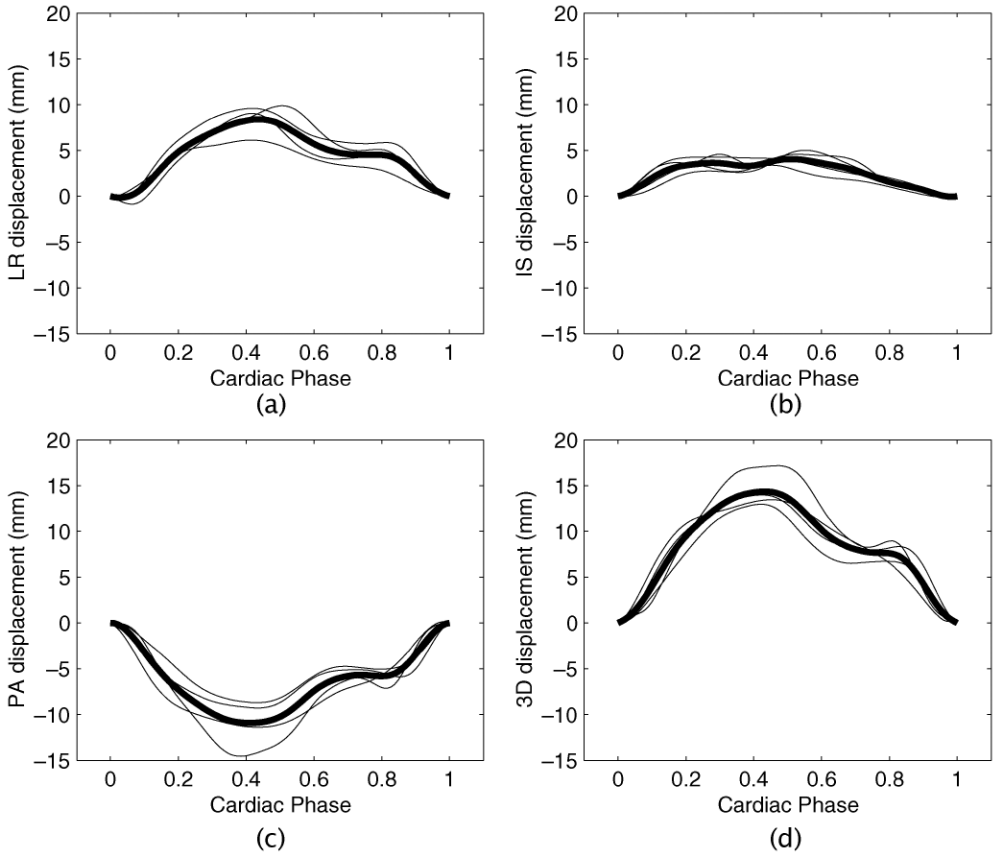

Fig. 1.

Displacement of the RCA origin during the cardiac contraction. The plots show individual results for four patients (thin lines) and the mean displacement (thick line). One-dimensional displacements are with respect to the patient's (a) left-right, (b) inferior-superior, and (c) posterior-anterior axes. Positive displacements are toward the left, inferior, and posterior, respectively. The shape of the 3-D magnitude displacement curve (d) has several features: 1) a large rapid systolic motion from $\chi = 0$ to $\chi \approx 0.4$; 2) a variable length end-systolic period of stasis at $\chi \approx 0.4$; 3) a rapid motion corresponding to early diastolic filling from $\chi \approx 0.4$ to $\chi \approx 0.6$; 4) a static period at mid-diastole (diastasis) from $\chi \approx 0.6$ to $\chi \approx 0.8$; 5) a rapid motion corresponding to the atrial contraction from $\chi \approx 0.8$ to $\chi \approx 1$. Individual patient variability affects the shape and duration of these features.

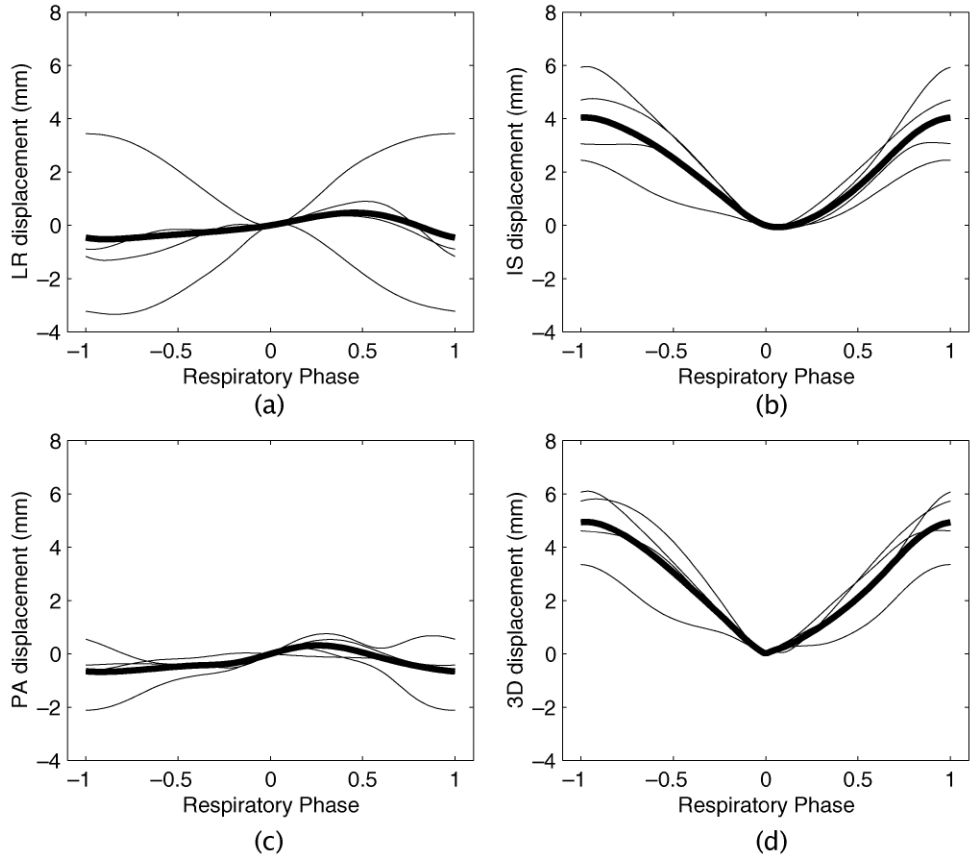

Fig. 2.

Displacement of the RCA origin during a tidal breathing cycle. The plots show individual results for four patients (thin lines) and the mean displacement (thick line). One-dimensional displacements are with respect to the patient's (a) left-right, (b) inferior-superior, and (c) posterior-anterior axes. Positive displacements are toward the left, inferior, and posterior, respectively. Since end-expiration was the reference state, the shape of the 3-D magnitude displacement curve (d) has a minimum at end-expiration ($\rho = 0$), and a maximum near end-inspiration ($\rho = \pm 1$).

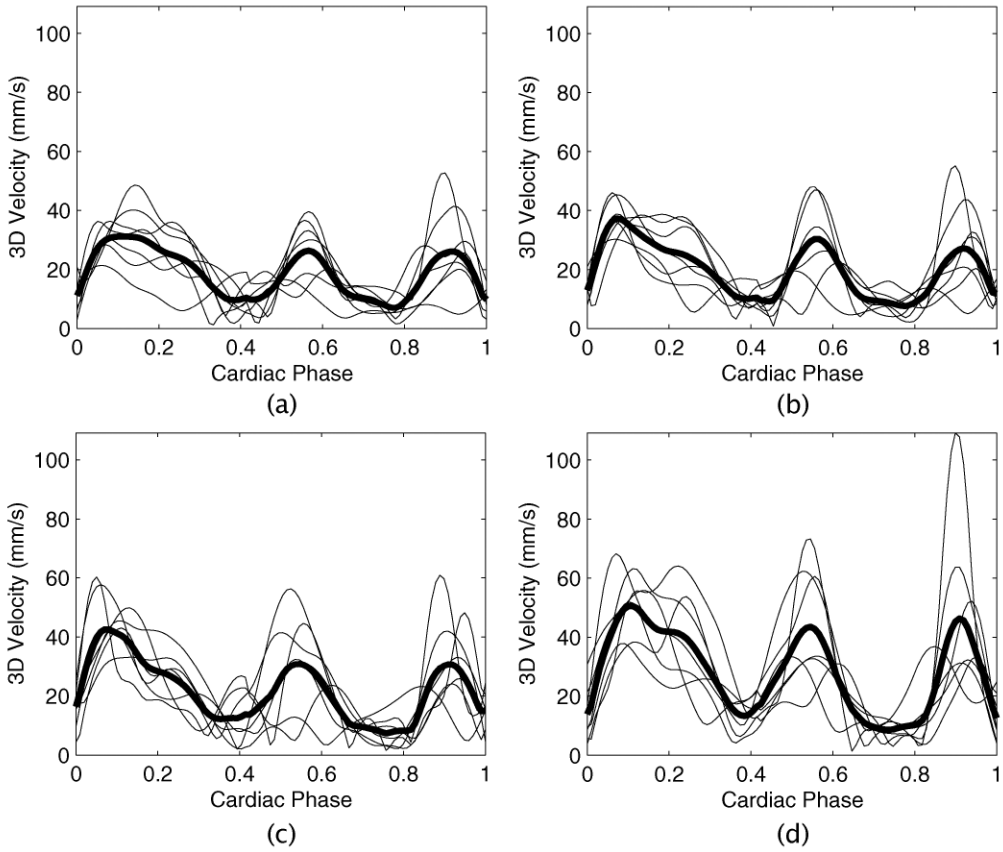

Fig. 3.

Velocity of the left coronary tree during the cardiac contraction. The plot shows individual results for seven patients (thin lines) and the mean velocity (thick line). Velocities are plotted at (a) the LM ostium, (b) the LM bifurcation, (c) a point on the LAD 5 cm from the LM ostium, and (d) a point on the LCx 5 cm from the LM ostium.

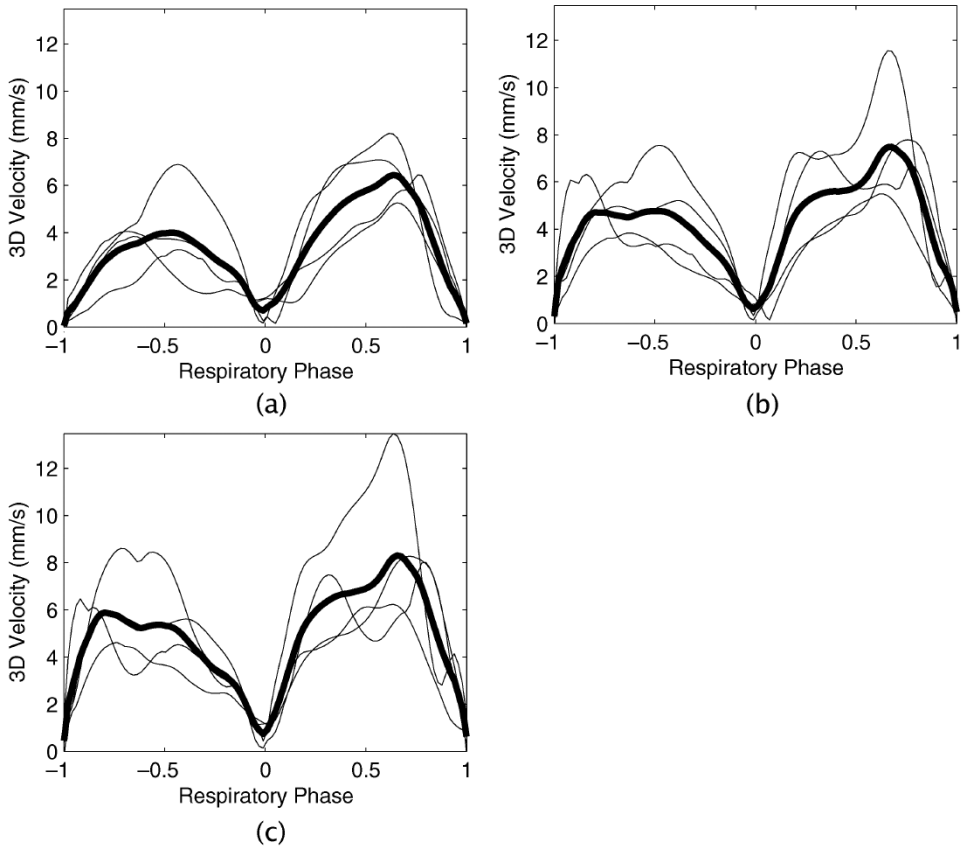

Fig. 4.

Velocity of the RCA during a tidal breath. The plot shows individual results for four patients (thin lines) and the mean velocity (thick line). Velocities are plotted at (a) the RCA ostium, (b) a point on the RCA halfway to the anterior margin, and (c) a point on the RCA at the anterior margin of the heart.

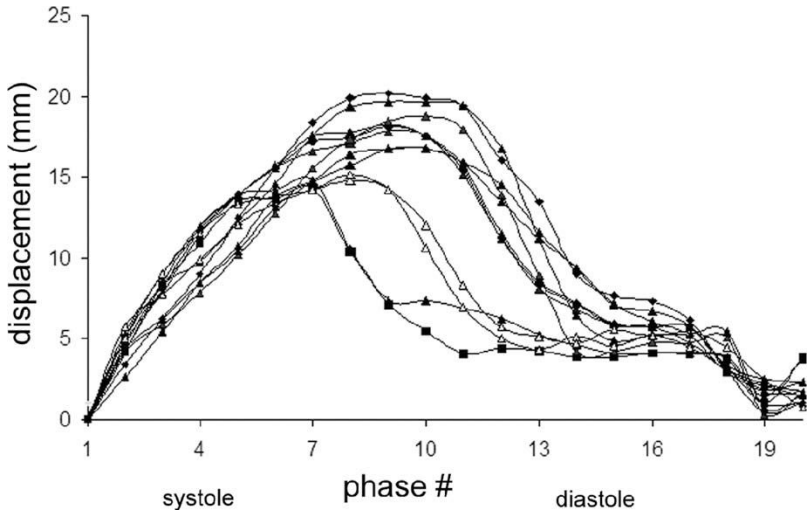

Fig. 5.

Displacement of the proximal RCA in 12 subjects as a function of the cardiac phase [14]. These measurements were made from 2-D breath held magnetic resonance images, and correlate well with results obtained in this study as shown in Fig. 1(d).

TABLE I

Maximum Displacement of Coronary Landmarks During a Cardiac Contraction in Millimeters (mm). 3-D=Three-Dimensional; LR=Left-Right; IS=Interior-Superior; PA=Posterior-Inferior. Positive Displacement is Towards the Left, Inferior, and Posterior, Respectively

Coronary Landmark	3D (mm)	LR (mm)	IS (mm)	PA (mm)
RCA_0	14.4 ± 1.9	8.7 ± 1.7	4.6 ± 0.3	−11.0 ± 2.6
$RCA_{.5AM}$	26.3 ± 3.1	15.0 ± 1.8	7.2 ± 1.6	−20.4 ± 4.0
RCA_{AM}	23.2 ± 1.6	12.3 ± 2.6	6.2 ± 1.7	−18.3 ± 3.2
LM_0	7.9 ± 2.2	4.8 ± 2.2	4.3 ± 1.1	−4.6 ± 1.6
LM_B	8.5 ± 1.7	5.3 ± 1.8	4.7 ± 0.6	−4.9 ± 1.5
LAD_5	9.6 ± 1.3	5.0 ± 2.3	5.7 ± 0.9	−4.8 ± 3.5
LCx_5	12.1 ± 2.4	6.8 ± 3.4	7.3 ± 1.9	−6.8 ± 1.8

TABLE II

Maximum Displacement of Coronary Landmarks During a Tidal Breath in Millimeters (mm). 3-D=Three Dimensional; LR=Left-Right; IS=Interior-Superior; PA=Posterior-Inferior. Positive Displacement is Towards the Left, Inferior, and Posterior, Respectively

Coronary Landmark	3D (mm)	LR (mm)	IS (mm)	PA (mm)
RCA_0	5.0 ± 1.3	−0.5 ± 2.8	4.1 ± 1.6	−0.4 ± 1.3
$RCA_{.5AM}$	6.4 ± 1.9	−0.3 ± 3.4	5.1 ± 2.1	−1.0 ± 2.5
RCA_{AM}	7.2 ± 2.2	−1.3 ± 1.6	5.9 ± 3.1	−2.1 ± 2.7
LM_0	4.6 ± 1.4	−0.4 ± 3.0	4.1 ± 1.0	−0.8 ± 1.1
LM_B	5.0 ± 1.6	−0.1 ± 3.0	4.3 ± 1.1	−0.8 ± 1.4
LAD_5	5.6 ± 2.1	0.1 ± 3.5	4.7 ± 1.8	−0.7 ± 1.9
LCx_5	6.3 ± 1.6	0.3 ± 2.8	5.6 ± 1.5	−0.6 ± 1.9

TABLE III

Maximum 3-D Velocity of Coronary Landmarks During a Cardiac Contraction in Millimeters per Second (mm/s)

Coronary Landmark	Systole (mm/s)	Diastolic Filling (mm/s)	Atrial Contraction (mm/s)
RCA_0	69.8 ± 13.8	41.1 ± 15.0	63.0 ± 21.4
$RCA_{.5AM}$	130.7 ± 19.4	70.4 ± 36.2	120.8 ± 46.7
RCA_{AM}	101.8 ± 13.4	60.1 ± 23.8	103.4 ± 40.7
LM_0	34.5 ± 8.8	27.9 ± 9.2	29.1 ± 13.8
LM_B	39.1 ± 5.4	32.6 ± 11.3	31.5 ± 13.9
LAD_5	47.5 ± 9.3	35.6 ± 12.6	36.8 ± 14.3
LCx_5	56.4 ± 10.1	46.7 ± 17.9	51.3 ± 28.3

TABLE IV

Maximum 3-D Velocity of Coronary Landmarks During a Spontaneous Tidal Breath in Millimeters per Second (mm/s)

Coronary Landmark	Expiration (mm/s)	Inspiration (mm/s)
RCA_0	4.5 ± 1.6	6.6 ± 1.3
$RCA_{.5AM}$	5.7 ± 1.6	8.0 ± 2.5
RCA_{AM}	6.4 ± 1.7	9.0 ± 3.1
LM_0	5.5 ± 2.0	6.0 ± 1.8
LM_B	5.7 ± 2.4	6.3 ± 2.0
LAD_5	7.6 ± 3.9	7.8 ± 3.0
LCx_5	6.9 ± 3.1	8.5 ± 4.3